

How to Cite:

Shamia, A. Y. M. ., Abd-Alhafez, A.-A., Al-qalshy, E. S., & Zouair, M. G. A. (2022). Therapeutic efficacy of time-dependent cetuximab on experimentally induced hamster buccal pouch carcinoma. *International Journal of Health Sciences*, 6(S5), 3431–3456.
<https://doi.org/10.53730/ijhs.v6nS5.9395>

Therapeutic efficacy of time-dependent cetuximab on experimentally induced hamster buccal pouch carcinoma

Ashraf Yehia Mohamed Shamia

Assistant lecturer, of Oral and Dental Pathology department, Faculty of Dental Medicine, Al-Azhar University, Palestine.

Corresponding author email: Dr_shamia@hotmail.com

Dr. Abd-Alshakor Abd-Alhafez

Lecturer, of Oral and Dental Pathology department, Faculty of Dental Medicine, (Boys), Al-Azhar University, Cairo, Egypt.

Email: Dr.ahmedshokry1@gmail.com

Dr. Emad Soliman Al-qalshy

Lecturer, of Oral and Dental Pathology department, Faculty of Dental Medicine, (Boys), Al-Azhar University, Cairo, Egypt.

Email: emadalqalshy.209@azhar.edu.eg

Prof. Mohamed Gomaa Attia Zouair

Professor of Oral and Dental Pathology department, Faculty of Dental Medicine, (Boys), Al-Azhar University, Cairo, Egypt.

Email: Dentistonline24@yahoo.com

Abstract---Purpose: This study aimed to determine the cetuximab therapeutic potential in the time-dependent fashion in experimentally induced hamster buccal pouch (HBP) carcinoma. Material and methods: Forty Syrian male hamsters were classified into four equal groups (G) of ten each. GI: The animals remained untreated to act as negative controls. The right pouches of animals in GII, GIII, and GIV were painted three times a week for 14 weeks (w)s with 7,12-dimethylbenz (a) anthracene (DMBA). GII: No additional treatment was administered. While, the animals in GIII and GIV were treated differently. Those in GIII received cetuximab intraperitoneally (IP) three intervals a week for three (w)s, whereas those in GIV received cetuximab IP three intervals for six (w)s. After the end of the experiment, the gross observations were made, and blood samples (2ml) were withdrawn from the inner canthus of the eye for analysis of whole white blood cells (WBCs) and oxidative stress markers

[glutathione (GSH) and malondialdehyde (MDA) levels]. All pouches were surgically bisected for preparation for Hematoxylin and Eosin (H&E) stain and immunohistochemistry (IHC) stain using epidermal growth factor receptor (EGFR). Other fresh tissue was used for DNA detection through a flow cytometry (FCM) test. Results: In this study, the results revealed some variability across the medicated Gs (GIII, GIV) contrasted to GII. There was a highly significant difference in DNA analysis (diploid, aneuploid, diploid S phase fraction (SPF), and aneuploid SPF) between GII and either GIII or GIV (p-value < 0.001). Additionally, there was a significant difference in DNA analysis between GIII and GIV. Conclusion: Cetuximab is a potentially effective immunotherapeutic agent, and has a time-dependent manner, in which cetuximab GIV (6 w) inhibits tumor progression in hamster buccal pouch (HBP) carcinoma than GIII (3 w). On the contrary, GII was highly significant than GIV regarding oxidative stress indicators.

Keywords---Cetuximab, EGFR, HBP carcinoma.

Introduction

Oral squamous cell carcinoma (OSCC) has been responsible for more than 800,000 new cases and 450,000 deaths. (1, 2). Regrettably, OSCC is linked with a high rate of morbidity and death, and despite significant progress in diagnosis and treatment options, the 5-year survival rate has not enhanced significantly. (3, 4) Moreover, the depth of invasion (DOI) as a predictor of cervical nodal metastasis and local recurrence in early stage of oral squamous cell carcinoma, also, has been a matter of interest. (5) These owing primarily to drug effectiveness issues, metastatic spread, and resistance (3, 4). Moreover chemobiological interaction including lipid peroxidation and antioxidant status in human as well as 7,12-dimethylbenz (a) anthracene (DMBA) induced hamster buccal pouch (HBP) carcinoma has been found. (6) Interestingly, the role of the epidermal growth factor receptor (EGFR) in the development and progression of head and neck squamous cell carcinoma (HNSCC) has been widely studied. Different malignant tumors in human exhibited different grades of aneuploidy that mostly correlated with the tumors histopathological behavior, the DNA content analysis involving general ploidy and S-phase fraction (SPF) is a powerful key indicator for tumor activity and malignancy during development of OSCC (7). Although controversy has been existed in the management of OSCC, chemotherapeutic treatment with cetuximab, carboplatin and paclitaxel have great interest (8, 9). On top of that, cetuximab enhanced the antitumor activity of several chemotherapeutic drugs in mouse xenograft models (10). They have only shown a minor advantage and, like standard chemotherapy, are susceptible to primary and secondary resistance, as well as several adverse effects have been reported, damage to normal cells mainly neurotoxicity and nephrotoxicity that limit its clinical use (11), which ultimately results in treatment failure (12). Cetuximab is a chimeric immunoglobulin G (IgG)-subclass monoclonal antibody that binds to the extracellular domain of the EGFR with higher affinity than the natural ligands EGF, blocking the activation of its intracellular domain and subsequent tyrosine kinase-dependent signal transduction pathway (13), also stimulates the internalization of EGFR, removing

the receptor from the cell surface and thus preventing its interaction with the ligand (14). Since it decreases the proportion of cells in S phase and increases that of G1 phase, facilitates apoptosis, decreases the capacity of DNA repair, and has an antiangiogenic effect (15, 16). Experimentally DMBA induced Oral carcinogenesis in golden Syrian hamsters has become a well-accepted and well-characterized experimental paradigm for various investigations including biochemical, histological, immunohistochemistry (IHC), and molecular alterations EGFR is a transmembrane glycoprotein member of the tyrosine kinase growth factor receptor family that regulates cell growth and proliferation (17). This receptor is overexpressed in up to 90% of HNSCC and has been associated with decreased survival (18). The accumulating evidence led to the evaluation of agents targeting the EGFR pathway in this tumor type. The effect of DMBA on various carcinoma models for mutagenic changes includes the involvement of several signaling pathways facilitating malignancy and cell proliferation, The over-expression and activation estrogen receptor- α (ER α), progesterone receptor (PR), and EGFR signaling pathways take place in mammary carcinoma (19). Thus, the primary aim of this study was to determine the therapeutic efficacy of time-dependent cetuximab as an anticancer therapy strategy in DMBA-induced HBP carcinoma, as well as the associated adverse events. The evaluation depends on the histological tumor tissue changes, IHC examination, blood analysis, and flow cytometry (FCM) studies.

Materials & Methods

Chemicals

DMBA (0.5%) was gathered from Sigma-Aldrich company, solubilized in paraffin oil. Cetuximab (C225, Erbitux Merck Serrano - Germany) was redispersed in phosphate-buffered saline (PBS) buffer (pH 7.4) and kept at 4°C to be used.

Animals

Forty Syrian male hamsters, weighing between 80 and 120g, and five weeks old. The experimental hamsters were kept in standard boxes with sawdust bedding in a controlled environment with humidity (30-40%), temperature (20 \pm 2°C), and light (12-hour light/12-hour dark). A healthy hamster walks regularly and smoothly, had bright, clear eyes, healthy skin, and a soft, lustrous coat devoid of parasites, wounds, dry spots, and swellings.

Experimental design

The animals were randomly categorized into four groups Gs after a week of adaptation. Each group had 10 animals. The right pouches of the animals in GII, GIII, and GIV were painted three times a week for 14 weeks with 0.5% DMBA in liquid paraffin by a number 4 camel's hairbrush (Fig. 1A) ,(20) whereas the animals in GI (negative control) were kept untreated. Following that, the animals in GII (positive control) underwent no other medication, whereas those in GIII (cetuximab-3w) received cetuximab 1 mg/animal IP via insulin syringe at 3-day intervals for 3 weeks. (21, 22) (Fig. 1B), whereas those in GIV (cetuximab-6w)

were injected IP by insulin syringe with cetuximab 1 mg/animal at 3 days intervals for 6 weeks.

General health examinations

The alterations in the animal's general health were monitored throughout the experiment. Hamsters that demonstrated any of the following signs (crowding in sneezing, anorexia, silence, corner, diarrhea, discharge from the nose or eyes, dampness around the tail, wheezing, and hair loss) of illness or disease were adapted.

Tumor volume measurement:

After termination of the experiment, gross observations of HBP mucosa were recorded (mucosal thickness, exudation, ulcers, and tumors). Then, the animals were euthanized, the right cheek pouch everted, and the diameter of each tumor was measured with a Vernier calliper (Fig.1C). The tumor volume, where the three diameters (mm) of the tumor are D1, D2 and D3, was calculated by the formula, $V_{mm3} = (4/3) \pi [(D1/2) (D2/2) (D3/2)].(23)$

Blood and serum analysis

At the experimental end and before animals euthanization, the animals were anesthetized using ethyl ether inhalation. Then, blood samples (2ml) were withdrawn from the inner canthus of the eye from each animal into a sterile tube (**Fig. 1D**) for total WBCs and oxidative stress markers GSH and MDA levels. The blood samples were collected in a heparinized tube, then immediately sent for blood counting using a fully automatic cell counter (Heco serc, Italy). The analysis was performed according to the manufacturer's instructions.(24)

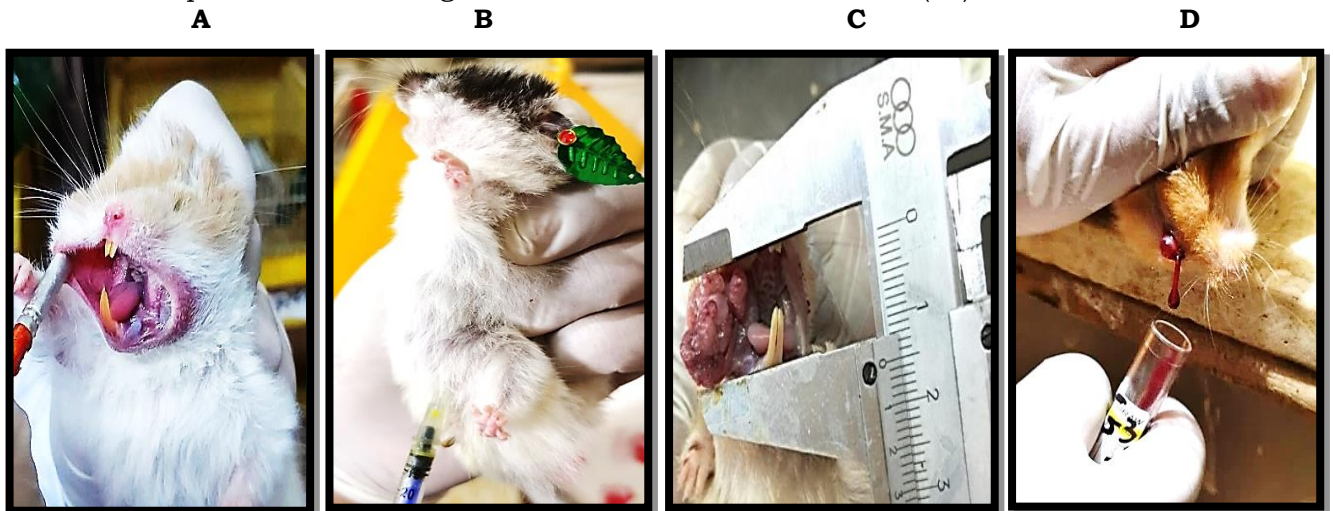


Fig. 1. Painting the HBP with DMBA (A), IP injection (B), and blood was withdrawn from the inner canthus of the eye (C). Calculating tumor volume using Vernier caliper (D).

Sample collection and preparation

The pouch on the right cheek was removed and bisected. For histological and immunohistochemical evaluation, one piece of fresh tissue was preserved in 10% neutral buffered formalin, treated normally, and preserved in paraffin blocks. The other fresh tissue sample was mechanically digested, immobilized, and subjected to FCM analysis.

Histopathological examinations

Utilizing a rotary microtome, 4 μm thick tissue sections were cut from paraffin blocks, processed, mounted on glass slides, and stained with Hematoxylin and Eosin (H&E) for light microscopic inspection.

Measurement of the depth of invasion (DOI)

The DOI of all surgical specimens was determined using the H&E slide. The DOI was calculated from the surface epithelium's basal layer to the deepest point of tumor infiltration. According to the American joint committee of cancer (AJCC), it is further characterized as less invasive at ≤ 5 mm, moderately invasive at 6-10 mm, and highly invasive at ≥ 10 mm(25) (**Fig.2**). The DOI was determined by a Leica QWIN V3 image analyzer computer system (Switzerland), which was operated via the Leica QWIN V3 software. This was done in Oral and Dental Pathology Department, Faculty of Dental Medicine (Boys-Cairo), Al-Azhar University, Egypt.

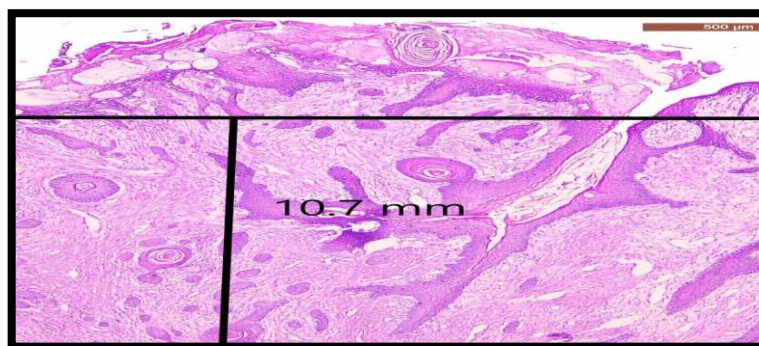


Fig. (2): Photograph of measuring the DOI, the greatest invasion was measured by dropping a “plumb line” from the horizon to the deepest invasive nest.

Immunohistochemical examination:(26)

Other tissue sections 4 μm were placed on positively charged slides. The sections were deparaffinized in xylene and rehydrated via graded ethanol (100%, 95% and 70%), each run for 5 minutes. The slides were then rinsed in distilled water and PBS, each for 5 minutes. The sections were enzymatic cells treated by immersion in the slide racks container with 0.1% of pepsin, prepared one hour early (Pepsin: 0.2g, Calcium chloride: 0.2g and distilled water: 200 ml), then immersed in a water bath for 30 minutes at 37°C in the hot oven, as enzymatic retrieval

methods. Slides were then cleaned in PBS, each for 5 minutes. Endogenous peroxidase activity was inhibited for 10 minutes at room temperature using 3% solution of hydrogen peroxide in methanol. Then, the samples were rinsed twice with PBS, each for 5 minutes, pH 7.2 to 7.6. Then, excess liquid was blotted around the tissues with filter paper. A serum block was applied to cover the specimen. The slides were incubated for 10 minutes at room temperature. The solution was drained and did not rinse after this step. To cover the tissue sections, two to three drops of the primary polyclonal IgG EGFR antibody at a dilution of 1:50 were applied. The slides were kept in the refrigerator overnight at 4°C. After that, the slides were rinsed in distilled water and then in PBS for 5 minutes. For 30 minutes at room temperature, the slides were thoroughly covered with biotinylated (secondary antibody), ready to use. Excess fluid was wiped around the tissues with filter paper after washing the slides three times in PBS for five minutes. The slides were thoroughly covered with peroxidase-labeled streptavidin and left at room temperature for 30 minutes before being rinsed in PBS.

The tissue slices were dyed with DAB for 2 minutes before being immersed in cold water to cease the reaction. Mayer's hematoxylin was used to counterstain the tissue sections for 1 minute before rinsing in tap water. The slides were soaked in xylene after being immersed in two variables of 95% alcohol accompanied by two modifications of absolute alcohol, each for three minutes. Before mounting, three three-minute washes were allowed. Each slide was immersed in xylene for 1 second before being mounted with DPX and covered with coverslips. On immunostained tissue sections, the proportion of positive cases and the localization of immunostaining within the tissues were analyzed using a light microscope. Furthermore, the percentage of EGFR-positive cells with immunostaining surface area was calculated using an image analysis computer system.

DNA cell cycle analysis for cancer cells:(27)

Tumor cell suspensions were stained with a DNA staining kit (Beckman Coulter, Fullerton, CA) according to the manufacturer's instructions and analyzed by FACSCaliber FCM. MODFIT, a DNA analysis tool, was used to analyze the data (Verity Software House, Inc., Topsham, ME, USA). The percentage of cells in each phase of the DNA cell cycle (G0/G1, S, and G2/M) was estimated using computer software for each sample. The diploid lesions had a single diploid peak that looked identical to the reference peak at (2N). An aneuploidy cell population was regarded present if a distinct peak, in addition to the G1 diploid peak, departed more than 10% from the diploid internal standard, or if the G1 itself diverged more than 10% from a corresponding G2/M peak.

Interpretation of DNA:(28)

The Y-axis represents the number of events (cells or nuclei), while the X-axis measures the intensity of fluorescence of propidium iodide bound to DNA. Tumors with a single G0/G1 peak with DI of 0.95 to 1.05 to the reference sample were classified as DNA diploids. If two distinct G0/G1 peaks were discovered, with an aberrant G0/G1 peak comprising at least 15% of the total occurrences and a

corresponding G2/M peak, the tumors were classified as DNA aneuploid. The relative DNA content was calculated by dividing the abnormal (aneuploid) G0/G1 peak by the mean channel number of the normal (diploid) G0/G1 peak. The ratio is represented by the acronym DI. Aneuploid was defined as a sample with a DI of less than 0.95 (Hypodiploid) or greater than 1.05 (Hyperdiploid). The DI was calculated using statistical methods and evaluated using a machine (**Fig. 3**).

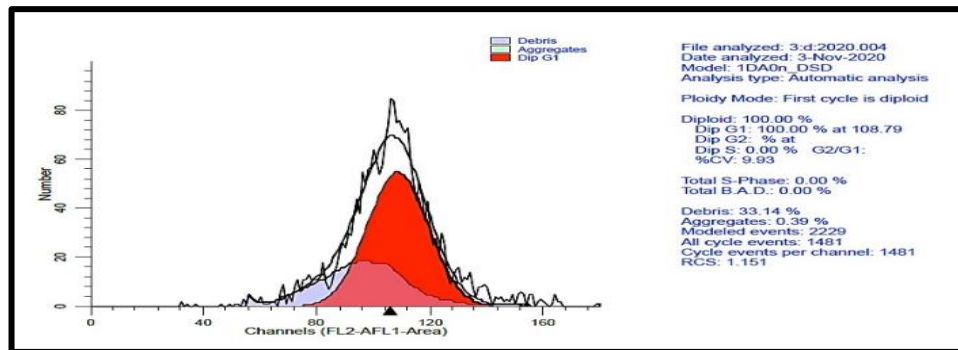


Fig.3. Interpretation of DNA histogram

Statistical analysis

The data were statistically examined, and the mean and standard deviation were calculated (SD). A one-way analysis of variance was performed using SPSS version 17.0 for Windows (ANOVA). With quantitative data and parametric distribution, ANOVA was utilized to differentiate between more than two separate groups, accompanied by post hoc analysis with the LSD test. To establish significance, the relevant p-values were used: $p < 0.05$: significant, $p > 0.05$: non-significant, and $p < 0.001$: extremely significant.

Results

Gross observations

GI examination revealed no obvious alterations, neither hair loss or skin ulcerations. The HBP was normal pale pink with no pathological or inflammatory signs, their buccal pouch length was from (5-5.5) cm (Fig. 4A). Those in **GII**, all hamsters demonstrated debilitation and observable hair loss with para-oral skin ulcerations. Large exophytic growths with prominent vascularity in the animals' pouches, in addition to eroded, and ulcerative areas with spontaneous bleeding were seen (Fig. 4B). The mean tumors volume measurement of tumor-bearing animals in ten animals in **GII** was 814.6 mm³ (620 – 1005 mm³), and the pouch length in **GII** recorded from (1.5-2 cm). The mean tumors volume measurement in those of **GIII** and **GIV** was 269.13 mm³ (230.4 – 310.2 mm³) and 247.18 mm³ (180.1 – 390.5 mm³), respectively. The pouch length in **GIII** recorded from 3-3.5cm (Fig. 4C) and in **GIV** was 3.5-4cm (Fig. 4D). Comparing the positive control group **GII** with the various treated groups **GIII** and **GIV** according to tumor volume, there was extremely significant difference (p value < 0.001). Contrarily, there was a non-significant difference between **GIII** and **GIV** (p -value = 0.728).

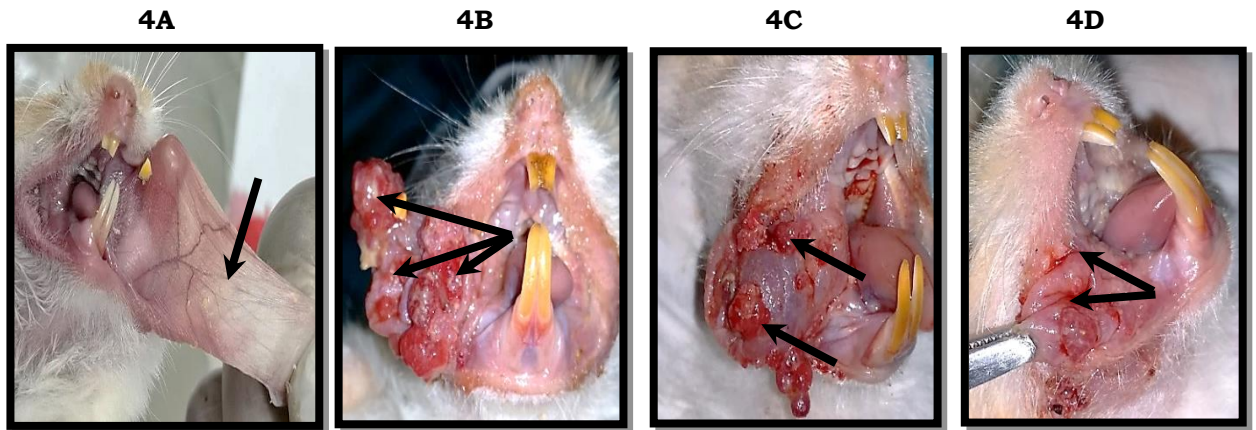


Fig. 4. A. GI's HBP indicates normal buccal pouch mucosa, which appeared pink in color with a smooth surface (arrow). 4B. GII's HBP demonstrates multiple exophytic papillary tumor masses surrounded by bleeding areas (arrows). 4C. GIII's HBP demonstrates medium size nodule with bleeding areas (arrows). 4D. GIV's HBP indicates a small size nodule with little bleeding areas (arrows)

Blood analysis results

Comparison between the studied groups regarding WBCs level:

Compared to GI, GII recorded, there was extremely significant difference (p-value < 0.001). Furthermore, there was non-significant difference between GII & GIII (p-value= 0.362) and significant difference between GIII & GIV (p value= 0.648). Also, there was a non-significant difference between GII and GIV (p-value = 0.648) (Table 1) and (Fig. 5).

Table 1: Contrasting between the studied groups regarding WBCs Level*

| | WBCs | | The P-value for post analysis using the LSD test | | | |
|----------------|-----------------------|---------|--------------------------------------------------|-------|-------|-------|
| | Mean ± SD | Range | G1 | GII | GIII | GIV |
| GI | 8.00 ± 2.35 | 4 – 12 | -- | 0.000 | 0.000 | 0.000 |
| GII | 14.00 ± 2.40 | 11 – 18 | 0.000 | -- | 0.362 | 0.648 |
| GIII | 13.00 ± 2.94 | 9 – 17 | 0.000 | 0.362 | -- | 0.648 |
| GIV | 13.50 ± 2.80 | 10 – 19 | 0.000 | 0.648 | 0.648 | -- |
| F | 12.605 | | | | | |
| P-value | <0.001 (HS) | | | | | |

*: WBCs count in the hamster is (Mean)×10³ cells/μl.

Comparison between the studied groups regarding MDA level

Compared to GI, GII recorded extremely significant difference (p-value < 0.001). Furthermore, there was non-significant difference between GII and either GIII or

GIV (p-value > 0.05) also there was non-significant difference between GIII and GIV (p-value > 0.05) (Table 2) and (Fig. 5).

Table 2 : Contrasting between the studied groups regarding MDA level:

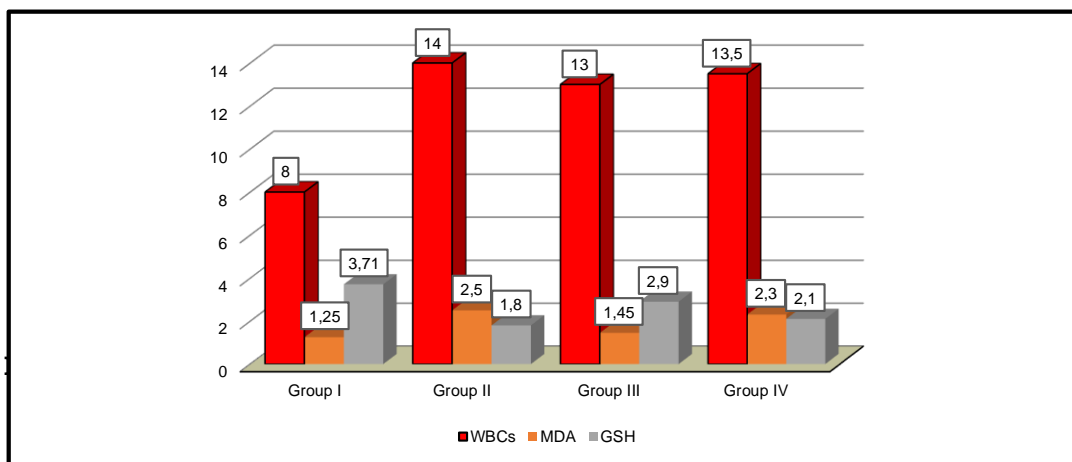
| | MDA | | The P-value for post analysis using the LSD test | | | |
|----------------|-----------------------|-----------|--------------------------------------------------|-------|-------|-------|
| | Mean ± SD | Range | G1 | GII | GIII | GIV |
| GI | 1.25 ± 0.54 | 0.4 – 2.1 | -- | 0.000 | 0.003 | 0.000 |
| GII | 2.50 ± 1.04 | 1.4 – 4.3 | 0.000 | -- | 0.156 | 0.476 |
| GIII | 2.10 ± 0.42 | 1.5 – 2.9 | 0.003 | 0.156 | -- | 0.476 |
| GIV | 2.30 ± 0.46 | 1.8 – 3.2 | 0.000 | 0.476 | 0.476 | -- |
| F | 4.874 | | | | | |
| P-value | <0.001 (HS) | | | | | |

Comparison between the studied groups regarding GSH level:

Compared to GI, GII recorded extremely significant difference (p-value < 0.001). Furthermore, there extremely significant difference between GII & GIII (p-value < 0.000) and non-significant difference between GIII & GIV (p value = 0.203) Contrarily, there was a significant difference between GII and GIV (p-value = 0.012) (Table 3) and (Fig. 5).

Table 3 : Contrasting between the studied groups regarding GSH level

| | GSH | | The P-value for post analysis using the LSD test | | | |
|----------------|-----------------------|-----------|--------------------------------------------------|-------|-------|-------|
| | Mean ± SD | Range | G1 | GII | GIII | GIV |
| GI | 3.71 ± 0.70 | 2.8 – 4.8 | -- | 0.000 | 0.011 | 0.000 |
| GII | 2.20 ± 0.95 | 1.2 – 3.9 | 0.000 | -- | 0.000 | 0.012 |
| GIII | 3.10 ± 0.34 | 2.4 – 3.6 | 0.011 | 0.000 | -- | 0.203 |
| GIV | 2.80 ± 0.28 | 2.4 – 3.1 | 0.000 | 0.012 | 0.203 | -- |
| F | 13.364 | | | | | |
| P-value | <0.001 (HS) | | | | | |



The **G1** exhibited a normal thin stratified squamous epithelium with minor keratinization, consisting of 2-3 layers of squamous cells. A subepithelial connective tissue and a muscle layer were discovered (Fig. 6A). **GII**: The overlying epithelium revealed multiple areas with dysplastic feature including basilar hyperplasia, hyperchromatism, loss of polarity, large nucleoli, altered N/C ratio, and cellular and nuclear pleomorphism (Fig. 6B). Destructive basement membrane with invasive epithelial islands into the underlying connective tissue. The mean DOI revealed 10.5mm. **GIII**: In tow hamsters out of 10 had epithelial dysplasia with top-to-bottom changes or carcinoma in situ. In contrast, the other eight had well-differentiated SCC that had not progressed to deeper parts. Distal necrosis was reduced, inflammatory infiltration was increased, and collagen fibers were increased (Fig. 6C). **GIV**: In three hamsters out of 10, exhibited epithelial dysplasia (hyperchromatism, changed N/C ratio, conspicuous nucleoli, cellular & nuclear pleomorphism, and numerous group cell keratinization). In comparison, the remaining seven hamsters exhibited well-differentiated SCC that did not extend to the deeper connective tissue, the connective tissue exhibited a reduction in distal necrosis, an elevation in inflammatory infiltration, and an elevation in the thickness of the striated muscle layer. At the same time, a few tumor masses were substituted by proliferating fibrous tissue with enhanced collagen deposition (Fig. 6D). The mean DOI in GIII and GIV revealed 3.5mm & 2.4mm respectively. There was extremely significant difference between treated groups (GIII and GIV) and positive control group (GII) (p value < 0.001). Furthermore, there was significant difference between GIII and GIV. (p value < 0.001)

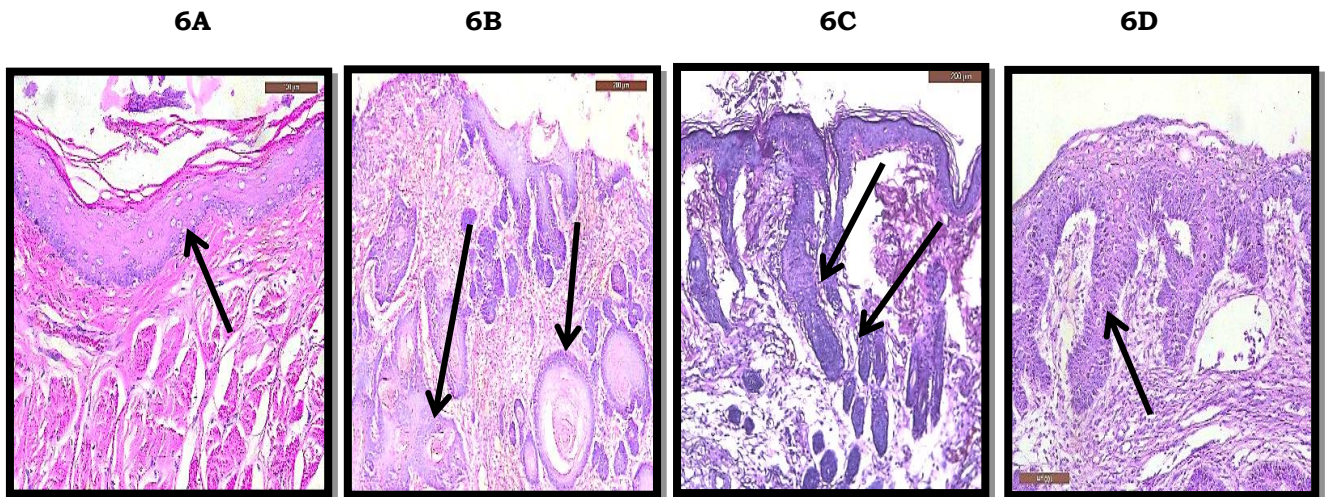


Fig. 6. A. G1 H&E stain demonstrates two to four layers of epithelium, superficial keratinized squamous cells, connective tissue layer, flattened rete ridges, muscular layer, and deep layer of loose areolar connective tissue (arrow). B. GII H&E stain shows well-differentiated SCC with deep penetration of several tumor islands into the underlying connective tissue and sub-epithelial inflammatory infiltrates (arrows). C. GIII H&E stain reveals nicely differentiated SCC (superficial invasion) (arrows). D. GV H&E stain shows extensive dysplasia with hyperkeratosis (arrow).

Table 4 : Contrasting between the studied groups regarding EGFR:

| | EGFR | | The P-value for post analysis using the LSD test | | | |
|----------------|-----------------------|-------------|--------------------------------------------------|-------|-------|-------|
| | Mean \pm SD | Range | G1 | GII | GIII | GIV |
| G1 | 0.82 \pm 0.10 | 0.65 – 0.96 | -- | 0.000 | 0.000 | 0.000 |
| GII | 53.40 \pm 4.38 | 47.1 – 61.1 | 0.000 | -- | 0.025 | 0.000 |
| GIII | 45.90 \pm 8.62 | 28.6 – 56.1 | 0.000 | 0.025 | -- | 0.001 |
| GIV | 32.50 \pm 6.82 | 23.7 – 50.1 | 0.000 | 0.000 | 0.001 | -- |
| F | 154.109 | | | | | |
| P-value | <0.001 (HS) | | | | | |

Immunohistochemical findings

G1: The IHC staining using EGFR antibody exhibited positive cytoplasmic and membranous expression, which was limited to basal and keratinous layers (Fig. 7A). (mean = 8.2%). **GII:** The IHC positive staining in the central part of both well-differentiated and moderately differentiated SCC. While the Peripheral cells of the invasive nests exhibited negative staining for EGFR (Fig. 7B). (mean =53.4%). **GIII:** The IHC positive staining throughout the overlying epithelium, and the central part of the invasive nests of well-differentiated SCC. With negative staining of Peripheral cells of the invasive nests (Fig. 7C). (mean =45.9 %). **GIV:** The IHC positive staining throughout the overlying epithelium, as well as in the central part of the invasive nests of well-differentiated SCC. Peripheral cells of the invasive nests exhibited negative staining for EGFR (Fig. 7D). (mean=32.5 %). There was extremely significant difference between both G1 and GII, also between GII and GIV (p-value < 0.001). There was a significant difference between GII & GIII (p-value = 0.002). Moreover, there was extremely significant difference between GIII and GIV (p-value = 0.001) (Table 4) and **(Fig. 8)**.

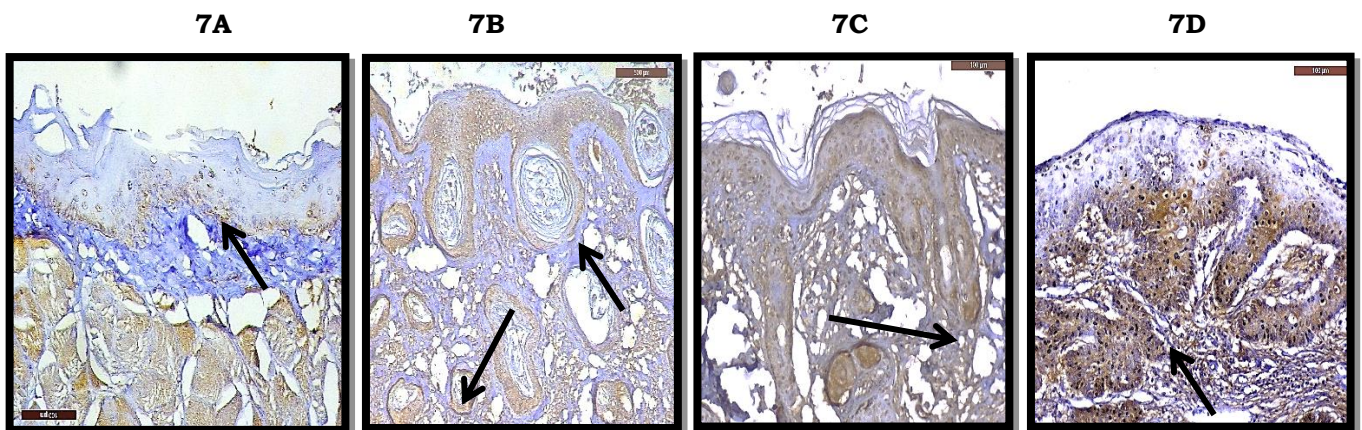


Fig. 7. A. EGFR IHC expression of G1 shows negative staining throughout the epithelial layers, except for positive cytoplasmic and membranous reactivity of some cells of the basal cell layer, and keratinous layer. Connective tissue shows a nonspecific reaction (arrow). B. EGFR IHC expression of GII indicates positive cytoplasmic and membranous staining during the overlying epithelium, as well as

in the invasive nests (arrows). C. EGFR IHC expression of GIII indicates positive cytoplasmic and membranous staining via the overlying epithelium, as well as in the invasive nests (arrow). D. EGFR IHC expression of GIV demonstrates positive cytoplasmic and membranous staining via the overlying epithelium, as well as in the invasive nests (arrow).

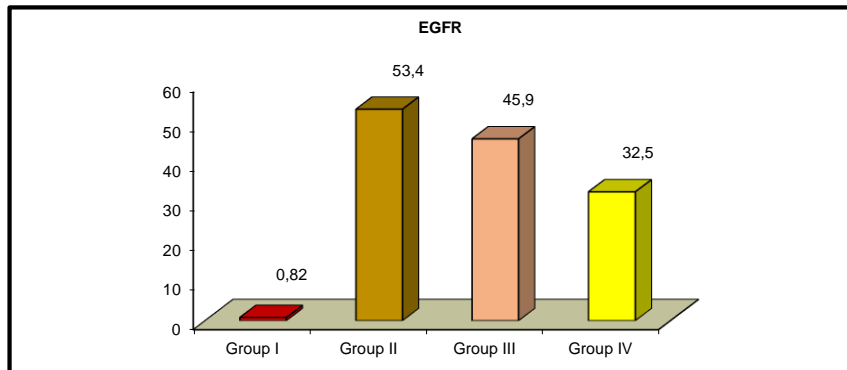


Fig. 8. Comparison between the studied groups EGFR

Detection of DNA cell cycle analysis for cancer cells by FCM

In GI, the normal HBPs mucosa were considered as standard that showed a single diploid peak (reference peak) expressing G0/G1 cells (2N) they had shown no cells in the S-phase or at G2/M peak (Fig. 9). The whole samples in GI were diploid and $DI = 0.95 < DI < 1.05$.

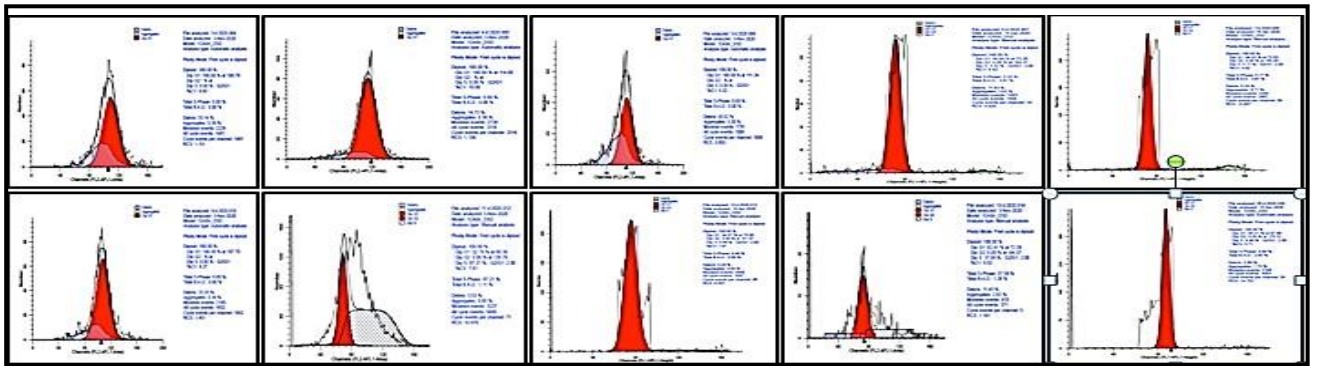


Fig. 9. DNA frequency histogram of diploid standard (normal tissue), showing a single G0/G1 peak and no SPF cells

In GII: Diploid DNA was identified in 20% of samples. The diploid lesions exhibited a single diploid peak similar to the reference peak (2N), while in 80% of samples DNA aneuploidy was observed. All aneuploid instances were hyperdiploid due to the exitance of additional stem lines to the **right** of the G0/G1 diploid peak, with DI values ranging from 1.06 to 1.12 with a mean of 1.1 (Fig. 10). The ploidy status (diploid versus aneuploid DNA pattern) between GI and GII was

statistically extremely significant (p -value < 0.001). Throughout the DNA ploidy GII revealed extremely significant aneuploid compared with diploid ($p= 0.001$). The SPF values for the cell cycles of the diploid GI recorded (0% - 5.62%), with a mean of 2.32%. In GII SPF was (1.93-25.94%) with a mean of 15.10% in diploid lesions., while the SPF of aneuploid lesions, ranged between 10.25-51.50%, with a mean of 26.60%. There was significant difference in the mean SPF value of group I and group II (p -value < 0.05).

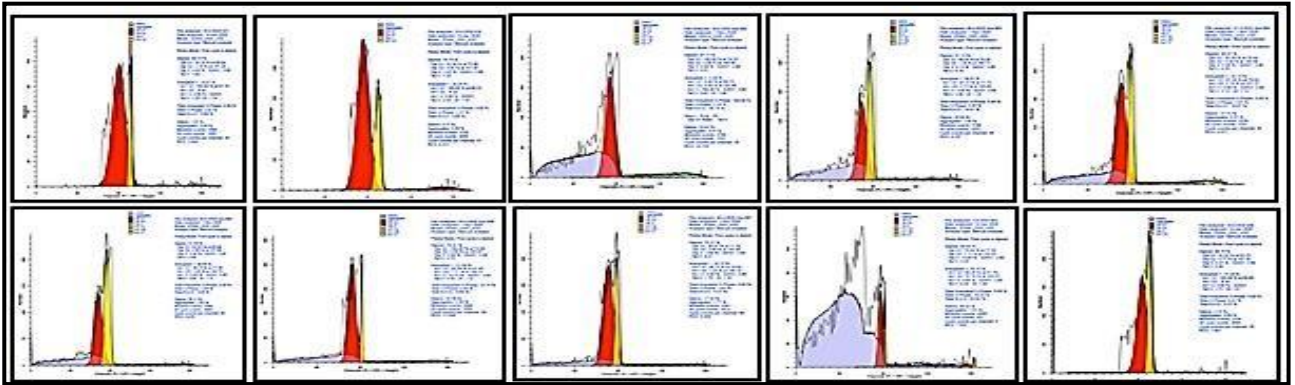


Fig. 10. DNA frequency histogram of GII

In GIII, (43.80%) DNA diploid was noticed. The diploid lesions demonstrated a single diploid peak equivalent to that of the reference peak (2N), and DNA aneuploidy was determined in (56.20%) of cases (Fig. 11). All aneuploid samples were hyperdiploid with DI varied from 0.9 1-1.09 with a mean of 1.02. The SPF values of the diploid lesions varied between 3.20%-45.30%, with a mean of 15.30%, and the SPF of the aneuploid lesions ranged between 4.50%-29.50%, with a mean of 16.80%.

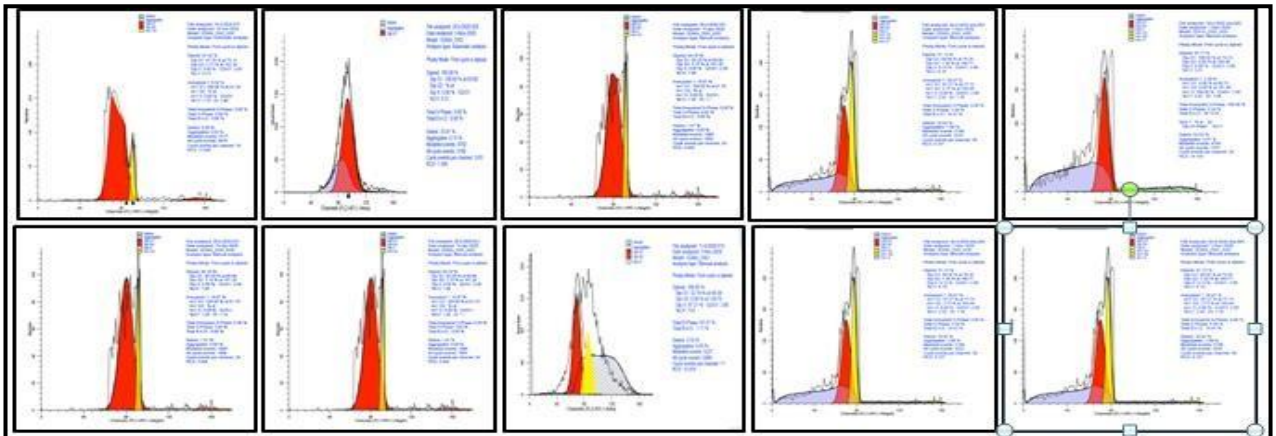


Fig. 11. DNA frequency histogram of GIII

In GIV, DNA diploid was determined in (49.40%) of cases. The diploid lesions indicated a single diploid peak at (2N) equivalent to that of the reference peak. While DNA aneuploidy was detected in (50.60%) of cases (Fig. 12). All aneuploid cases were hyperdiploid with DI varied from 1.01-1.08 with a mean of 1.05. The SPF values of the diploid lesions varied between 13.40% and 42.30%, with a mean of 14.40%, and the SPF of the aneuploid lesions varied between 5.50% and 42.50%, with a mean of 19.70 %. There was non-significant difference in the ploidy state (diploid and aneuploid DNA pattern) furthermore, the SPF values of diploid and aneuploid, either in GIII or GIV with (p-value > 0.05).

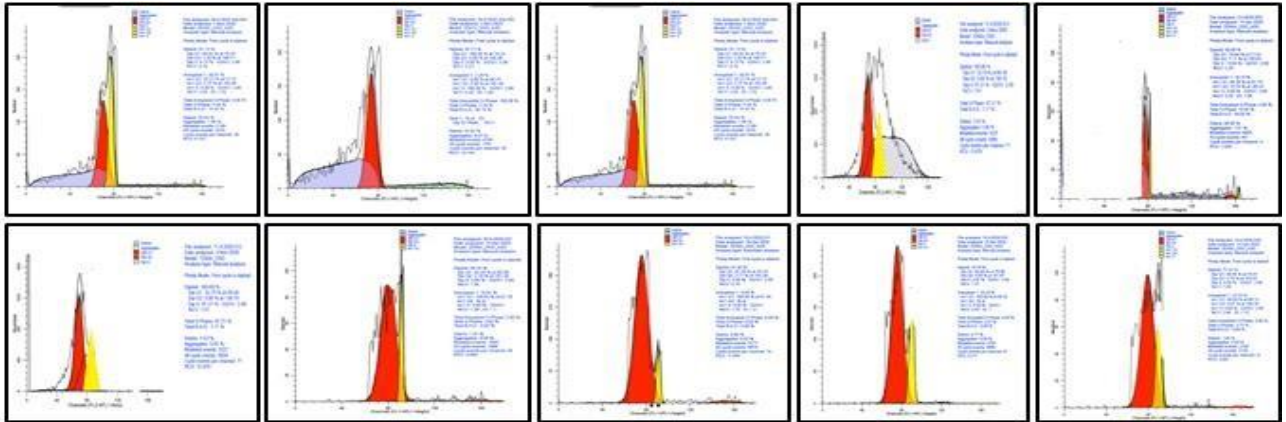


Fig. 12. DNA frequency histogram of GIV

Discussion

Oral cancer is one of the most disfiguring kinds of cancer. Despite the significant advancement in oral cancer treatment strategy, it remains a major induction of morbidity in human populations. Using the hamster cheek pouch system of the oral carcinogenesis model is beneficial for a deeper understanding of cancer biology, prevention, and treatment. The results of tumor volume, WBCs analysis, oxidative stress markers, H&E stain, IHC staining utilizing EGFR antibody and DNA cell cycle analysis for cancer cells by FCM evaluation showed variable insights.

In the present study, GII revealed noticeable systemic debilitation in all animals, in addition to perioral alteration and HBP tumor growth compared to GI. The latter was distinguishable by the results of the volume of tumor-bearing pattern (620 – 1005 mm³). Also, a decrease in the pouch length in GII (1.5-2 cm) compared to that of GI (5 cm) due to necrosis in the distal end of the pouch. Generally speaking, The results in GII are in consistence with those reported by other investigators (29, 30) These observations are mainly due to the strong toxic DMBA effect.(31)

In the present study, both GIII and GIV showed a relatively slight improvement in the animal's general health, The pouch length in GIII recorded from (2.5-3cm) and in GIV (3-3.5cm) was increased compared to GII (1.5-2cm) due to marked decrease of distal necrosis and inflammatory infiltration, furthermore, the mean tumors volume measurement in those of GIII and GIV was (230.4 – 310.2 mm³)

and (180.1 – 390.5 mm³), respectively, was decreased compared to GII (620- 1005 mm³). there was extremely significant difference (p value < 0.001). Contrarily, there was a non-significant difference between GIII and GIV (p-value = 0.728). These results were in line with other studies.^(32, 33) The non-responsiveness of cetuximab as a single agent may be caused by multiple intrinsic and extrinsic/acquired resistance mechanisms. In the case of OSCC, many tumors remain non-responsive to cetuximab in which the single-agent response rate of this drug is less than 15%. Nevertheless, cetuximab is known to provide a clinical benefit when used either in conjunction with radiation or in combination with chemotherapy.⁽³²⁻³⁵⁾ From a clinical point of view, Lu et al. (2007)⁽³⁶⁾ reported that acquired resistance occurs after an initial response to therapy and eventually all OSCC patients will relapse or become insensitive to further cetuximab therapy.

In the present study, GII revealed increase in total WBCs (14x10³ cells/ μ l) compared to that of GI (8x10³ cells/ μ l), this reflected by extremely significant difference (p-value < 0.001), this is in line with that reported by Khan et al (2022) ⁽³⁷⁾ This indicated the high local & systemic toxicity of DMBA in the hamster animal model.^(22, 28, 38) Similarly, Leucocytosis is prevalent in individuals with progressive OSCC. as Tumor-related leukocytosis this results explained hematopoietic colony- stimulating factors and inflammatory cytokines Production of cytokines, chemokines and granule proteins promotes, which promotes tumor growth, angiogenesis, and increase its metastasis potential. ^(39, 40)

When utilizing immunological therapy cetuximab in GIII, the current study, revealed decrease total WBCs (13x10³ cells/ μ l) compared to that of GII (14x10³ cells/ μ l), this with non-significant difference between GII and GIII (p value = 0.362) and GIV revealed decrease total WBCs (13.5x10³ cells/ μ l) compared to that of GII (14x10³ cells/ μ l), this reflected by significant difference between GII and GIV (p value = 0.648). Chen et al (2014)⁽⁴¹⁾ concluded the occurrence of leukocytosis (WBCs >15 \times 10 cells/uL)⁽⁴²⁾ in OSCC during the course of the therapy adversely impacts survival. Granger et al (2009)⁽⁴³⁾ enrolled 758 cancer patients with extreme leukocytosis (WBC >40 \times 10 cells/uL) during cancer therapy. They are also recruited to tumor microenvironment during radiotherapy, inducing angiogenesis that could offset treatment's effectiveness.^(39, 40)

In the current study, GII showed decrease in GSH level (2.20mmol/L) compared to that of GI (3.71 mmol/L), while GII showed an increase in MDA level (2.50 mmol/L) compared to that of GI (1.25 mmol/L). These findings were realized by extremely significant difference between GI and GII in both levels (p-value < 0.001). These results are consistent with those of other researchers.⁽⁴⁴⁻⁴⁶⁾ Glutathione and glutathione peroxidase have been reported to have a regulatory effect on cell proliferation. Increase in glutathione peroxidase and reduced glutathione could account for lowered oxidative stress. DMBA elicits its carcinogenic response via excessive generation of ROS, induction of chronic inflammation and excessive oxidative DNA damage.⁽⁴⁷⁻⁴⁹⁾ In previous studies on the DMBA model, the rats treated with DMBA were characteristic with the depletion of endogenous antioxidants such as MDA, SOD, CAT and TAC. This indicates poor antioxidant status in rats treated with DMBA.^(44, 45)

Furthermore, the amount of H₂O₂ produces tumor formations glutathione peroxidase and glutathione co-substrates are pivotal role in balancing of cellular integrity due to their changes or regulatory causes of cell proliferation. Early findings registered that development of cancer tissues rapidly requested from original mucosa and blood vessel transfusion to reach their nutrient deficiency as well as for fast and unlimited growth.⁽⁵⁰⁾ Overproduction of ROS within tissues can damage DNA and possibly contribute to mutagenesis and carcinogenesis. However, organisms have an array of potent adaptive antioxidant defense mechanisms [enzymatic antioxidants: superoxide dismutase (SOD), catalase (CAT) and glutathione peroxidase (GPx) and non-enzymatic antioxidants: reduced glutathione (GSH), vitamin C and vitamin E within the cells, to combat the deleterious effects of ROS- mediated oxidative damage.⁽⁵¹⁾

In the current study, GSH results of GIII (3.10mmol/L) and GIV(2.80mmol/L), this reflected by extremely significant difference between GIII & GII (p-value< 0.000) and non-significant difference between GIII & GIV (p value = 0.203) Contrarily, there was a significant difference between GIV and GII(p-value = 0.012) This result is in agreement with that of other investigators.^(52, 53) Lu et al (2016)⁽⁵⁴⁾, reported cetuximab downregulates of ASCT2 and thereby inhibits intracellular uptake of glutamine and subsequent biosynthesis of glutathione. Ozkan et al (2019),⁽⁵⁵⁾ revealed that, treatments of cetuximab were found to increase GSH activity in the cell lines. Because, cetuximab induced oxidative stress producing reactive oxygen species in cells.

In the current study, MDA results of GIII(2.10 mmol/L) and GIV(2.30 mmol/L) showed non-significant difference between GII and either GIII or GIV (p value > 0.05). This result is in agreement with that of other investigators.^(52, 56) Yang et al (2021)⁽⁵⁶⁾ results indicated that cetuximab decreased the activation of Nrf2/HO-1, which could in turn increased RSL3-induced lipid ROS and MDA levels.

In the present study, the histopathological findings, using H&E stain, GII revealed a development of diverse patterns of invasive SCC (50 % well-differentiated and 50 % moderately differentiated) that expanded into deeper areas of connective tissue (C.T) (DOI=10.5mm). These results in line with previous ones reported that 100% tumor growth occurred after 14 weeks of painting DMBA alone on the hamster's cheek pouches.^(31, 57) This could be due to proclivity for carcinogenesis since it is metabolized by phase I enzymes such as cytochrome P450 to its final carcinogenic metabolite, dihydrodiol epoxide, which damages DNA, this in turn causing mutation and cancer.⁽⁵⁸⁾ Furthermore, ROS has been implicated throughout phases of carcinogenesis (promotion, initiation, and progression). ROS can cause DNA damage, proto-oncogenes stimulation, tumor suppressor genes suppression, all of which can lead to neoplastic transformation.⁽⁵⁹⁾ Contrastingly, in the study conducted by Hussein et al (2018)⁽⁶⁰⁾ only 66.67% of the hamsters developed oral tumors, and that could be attributed to the different solvent material.

The histopathological findings in GIII and GIV displayed that 90% of the hamsters have less invasive well-defined SCC without spread to deeper areas, DOI in GIII and GIV were 3.5 and 2.4mm, respectively. These results, compared to GII, reflected extremely difference between (GIII and GII) and (GIV and GII) (p-value <0.001). They were in line with another study Boeckx et al (2013).⁽³²⁾ This could

be because cetuximab does not work as a single agent because it has multiple internal and external resistance mechanisms. There are many tumors that are not responding to cetuximab, which means that the single-agent response rate of this drug is less than 15%, which is true for OSCC. Cetuximab, on the other hand, is beneficial when used with radiation or chemotherapy.^(32, 61) People who work in the field say that after an initial response to treatment, the body learns to become resistant to the drug. Eventually, all OSCC patients will relapse or become intolerant to more cetuximab treatment.⁽³⁶⁾

In the present study, using IHC staining, GII revealed positive membranous-cytoplasmic expression of EGFR (53.4%) in contrast to GI that showed positive nuclear expression (8.2 %) with restriction to the basal and keratinous layer, this reflected by extremely significant expression (p-value < 0.001). These findings agree with those of others.⁽⁶²⁻⁶⁴⁾ Numerous studies have indicated that when OSCC cells were compared to the normal epithelium, EGFR was overexpressed, which was assumed to have an effect on cell proliferation and survival in OSCC.⁽⁶²⁻⁶⁶⁾ These antibodies detected epitopes in the extracellular region near the ligand-binding domain, the intracellular domain, the membrane-proximal extracellular region, and the phosphotyrosine autophosphorylation site of the EGFR tyrosine kinase domain. In OSCC, identifying the EGFR intracellular domain was linked to a poor outcome. Detection of the EGFR extracellular domain revealed no clinical correlation. According to OSCC research, the EGFR-mediated PI3K/Akt/mTOR signaling pathway stimulates inflammation, proliferation, angiogenesis, and metastasis.^(67, 68) In summary, phosphorylated EGFR tyrosine residues activate downstream PI3K/Akt/mTOR signaling pathways, which control NF- κ B activity in response to I κ B α kinase (IKK)-dependent I κ B α phosphorylation and degradation.⁽⁶⁹⁾ Phosphorylated mTOR appears to operate as a negative regulator of the tumor suppressors p53, p21(WAF1/CIP1), and Gsk-3 via stimulating the MDM2 signaling pathway.^(70, 71) Contrarily other studies, found no correlation between EGFR expression and tumor behavior when anti-EGFR extracellular domain antibodies.⁽⁷²⁻⁷⁴⁾

There was no difference in the area percentage of EGFR across different degrees of OSCC differentiation in our investigation, which is consistent with Ramu et al (2018).⁽⁷⁵⁾ This finding may imply that the level of differentiation of malignant keratinocytes is unrelated to EGFR. Although Sarkis et al (2010)⁽⁶³⁾ and Theocharis et al(2017)⁽⁷⁶⁾ believe that a modification in the regulation of cell proliferation is indicated by an elevation in the area percentage of EGFR, the number of cells damaged is the key sign of altered cell proliferation.

GIII and GIV revealed positive membranous-cytoplasmic expression of the EGFR (45.9% -32.5%) respectively, which was found in all over the epithelium and in the middle of well-differentiated SCC nests. These findings were realized by significant different GIII and GII (p-value = 0.002), and extremely significant difference between GIV and GII (p-value <0.001), this is in line with other studies.⁽⁷⁷⁻⁷⁹⁾ This could explain as cetuximab blocked the activity of EGFR in cells that had a lot of EGFR auto-phosphorylation at the start of the cell, even though the cells did not have a lot of EGFR expression. EGFR signaling and how well EGFR suppression works are also based on other factors, like EGFR mutations and polymorphisms in the downstream pathways.^(77, 80, 81)

Some studies, in lung and colon cancer cells, have looked into the possible reason why cetuximab is not working, and they found that activating some pathways could make EGFR inhibitors less effective, cancer cells had more extracellular signal-regulated kinase (MEK/ERK1/2) activity, making them more resistant to EGFR inhibitors. If the Akt signaling pathway is turned on, it will be more difficult for cetuximab to work for people with colon cancer Yonesaka et al (2011).^(82, 83) There was more activity in the MEK/ERK1/2 and Akt signaling pathways after medication with cetuximab, which could be because cetuximab does not work for people with OSCC.⁽⁸⁴⁾ also found a link between increased EMT markers and cetuximab resistance in 20 pre- and post-cetuximab OSCC biopsy samples. As a result, inhibiting EGFR/PI3K/Akt/mTOR phosphorylation is a promising method for preventing the carcinogenic potential of oral cancer. In DMBA-induced HBP carcinoma, gramine treatment reduces phosphorylation of EGFR tyr1068, PI3K tyr458, Akt ser473, mTOR ser2448, and IKK α / β ser176/180 residues, accompanied by reduction of IB ser32 phosphorylation, impairing NF- κ B p50 and p65 activities.⁽⁸⁵⁾

In the present study, GI (normal HBPs mucosa) as a reference, had a single diploid peak reflecting G0/G1 cells (2N), that all animals were diploid at the typical diploid peak. GII revealed 80% of sample had aneuploid DNA patterns, and 20% had diploid DNA patterns, all sample of aneuploidy were hyperdiploid (DI-1.1). The difference in ploidy status in GII (diploid versus aneuploid DNA pattern) and between GI and GII was statistically extremely significant (p-value < 0.001). These results corroborate with those of others denoting that DNA aneuploidy has a greater incidence of aneuploidy in breast,⁽⁸⁶⁾ and oral carcinogenesis.^(7, 87)

The present study revealed that aneuploid lesions have higher SPF (26.60%) versus the diploid one (15.10%), with statistically significant difference (p-value < 0.05). The mean SPF in our study is comparable to previously published values for FCM-determined SPF in HNC.⁽⁸⁸⁾ These results are consistent with several authors reported, that the SPF was significantly higher in aneuploid OSCC tumors than in diploid carcinomas and it a better indicator of tumor aggressiveness and predicting disease prognosis than the DNA ploidy.⁽⁸⁹⁾ El-Deftar et al (2012),⁽⁹⁰⁾ reported that the SPF aneuploid tumors were substantially more prevalent than diploid cancers. Contrastingly Zahran et al (2018)⁽⁹¹⁾ found that all diploid tumors have S-phase percentage less than those of the lowest aneuploid cell line but with no significant difference.

In the present study, diploid DNA in GIII and GIV instances revealed (43.80% and 49.40%) respectively. At the same time, DNA aneuploidy revealed (56.20% and 50.60%) respectively. These findings reflected extremely significant difference (p-value <0.001), either in GIII and GII or GIV and GII, all cases of aneuploidy in GIII and GIV were hyperdiploid, with DI mean (1.02- 1.05) respectively.

The SPF values in GIII and GIV for diploid (15.30% - 14.40%) respectively, while for aneuploid lesions SPF (16.80% - 19.70%) respectively. These findings according to SPF diploid reflected non-significant difference either in GII and GIII or GIV (p-value = 0.883- 0.608) respectively. Contrastingly findings according to SPF aneuploid reflected extremely significant difference either in GII and GIII or GIV (p-value = 0.000) These findings corroborate those of Otsuka et al (2019),⁽⁹²⁾

who discovered that tumors with low aneuploidy scores contained considerably more immune cells positive for CD8, Foxp3, and PD-1. The existence of these inflammatory markers suggests that tumors with low levels of aneuploidy may be more immunogenic than cancers with high levels of aneuploidy, which may lead to enhanced responses to immune checkpoint suppression. ⁽⁹³⁾

Conclusions

Cetuximab has a time-dependent manner a potentially effective immunotherapeutic agent, in which 6w treatment significantly inhibits tumor progression in HBP carcinoma compared to 3w treatment. On the contrary, GII was highly significant than GIV regarding oxidative stress indicators.

Conflicts of interests: The authors declare no conflicting financial interests.

Data Availability: The Data presented in this study are available on request from the corresponding author.

Funding: This research did not receive any specific grant from funding agencies in the public, commercial, or not-for-profit sectors.

Institutional review board statement

The National Research Council's Guide for the Care and Use of Laboratory Animals have been followed. All experiments were approved by ethical committee of Faculty of Dental Medicine (Boys Cairo), Al-Azhar University, Egypt (Ethical Code No. 489/2302) #

References

1. Ma H, Liu C, Zhang S, Yuan W, Hu J, Huang D, et al. miR-328-3p promotes migration and invasion by targeting H2AFX in head and neck squamous cell carcinoma. *Journal of Cancer*. 2021;12(21):6519.
2. Zawam HH, Selim A, Osman NO, Edesa W. Factors Influencing the Response Rate and Survival of Testicular Germ Cell Tumors: A Single Institution Experience from Egypt. *Research in Oncology*. 2021;17(2):66-72.
3. Ghantous Y, Bahouth Z, El-Naaj IA. Clinical and genetic signatures of local recurrence in oral squamous cell carcinoma. *Archives of oral biology*. 2018;95:141-8.
4. Yanamoto S, Umeda M, Kioi M, Kirita T, Yamashita T, Hiratsuka H, et al. Multicenter retrospective study of cetuximab plus platinum-based chemotherapy for recurrent or metastatic oral squamous cell carcinoma. *Cancer chemotherapy and pharmacology*. 2018;81(3):549-54.
5. Faisal M, Abu Bakar M, Sarwar A, Adeel M, Batool F, Malik KI, et al. Depth of invasion (DOI) as a predictor of cervical nodal metastasis and local recurrence in early stage squamous cell carcinoma of oral tongue (ESSCOT). 2018;13(8):e0202632.
6. Anbalagan V, RAju K, ShAnMugAM MJJoc, JCDR dr. Assessment of lipid peroxidation and antioxidant status in vanillic acid treated 7, 12-

- dimethylbenz [a] anthracene induced hamster buccal pouch carcinogenesis. 2017;11(3):BF01.
7. Hussein AM, El-Sheikh SM, Attia MA, Ramadan OR, Omar EM, Gaber AHJEDJ. Analysis of DNA ploidy and S-phase fraction in relation to development of oral squamous cell carcinoma: an experimental study. 2019;65(3-July (Oral Medicine, X-Ray, Oral Biology & Oral Pathology)):2447-55.
 8. Enokida T, Ogawa T, Homma A, Okami K, Minami S, Nakanome A, et al. A multicenter phase II trial of paclitaxel, carboplatin, and cetuximab followed by chemoradiotherapy in patients with unresectable locally advanced squamous cell carcinoma of the head and neck. *Cancer medicine*. 2020;9(5):1671-82.
 9. Peng W, de Bruijn HS, Ten Hagen TL, van Dam GM, Roodenburg JL, Berg K, et al. Targeted photodynamic therapy of human head and neck squamous cell carcinoma with anti-epidermal growth factor receptor antibody cetuximab and photosensitizer ir700dx in the mouse skin-fold window chamber model. *Photochemistry and Photobiology*. 2020;96(3):708-17.
 10. Bauman JE, Duvvuri U, Gooding WE, Rath TJ, Gross ND, Song J, et al. Randomized, placebo-controlled window trial of EGFR, Src, or combined blockade in head and neck cancer. 2017;2(6).
 11. Kitai Y, Matsubara T, Yanagita M. Onco-nephrology: current concepts and future perspectives. *Japanese journal of clinical oncology*. 2015;45(7):617-28.
 12. Hosseinian S, Hadjzadeh M-A-R, Roshan NM, Khazaei M, Shahraki S, Mohebbati R, et al. Renoprotective effect of *Nigella sativa* against cisplatin-induced nephrotoxicity and oxidative stress in rat. *Saudi journal of kidney diseases and transplantation: an official publication of the Saudi Center for Organ Transplantation, Saudi Arabia*. 2018;29(1):19-29.
 13. Gillison ML, Trotti AM, Harris J, Eisbruch A, Harari PM, Adelstein DJ, et al. Radiotherapy plus cetuximab or cisplatin in human papillomavirus-positive oropharyngeal cancer (NRG Oncology RTOG 1016): a randomised, multicentre, non-inferiority trial. 2019;393(10166):40-50.
 14. Giordano G, Remo A, Porras A, Pancione MJC. Immune resistance and EGFR antagonists in colorectal cancer. 2019;11(8):1089.
 15. Peng W, de Bruijn HS, Ten Hagen TL, van Dam GM, Roodenburg JL, Berg K, et al. Targeted photodynamic therapy of human head and neck squamous cell carcinoma with anti-epidermal growth factor receptor antibody cetuximab and photosensitizer ir700dx in the mouse skin-fold window chamber model. 2020;96(3):708-17.
 16. Taberna M, Oliva M, Mesía R. Cetuximab-containing combinations in locally advanced and recurrent or metastatic head and neck squamous cell carcinoma. *Frontiers in oncology*. 2019;9:383.
 17. Ang KK, Berkey BA, Tu X, Zhang H-Z, Katz R, Hammond EH, et al. Impact of epidermal growth factor receptor expression on survival and pattern of relapse in patients with advanced head and neck carcinoma. 2002;62(24):7350-6.
 18. Gettinger SN, Horn L, Gandhi L, Spigel DR, Antonia SJ, Rizvi NA, et al. Overall survival and long-term safety of nivolumab (anti-programmed death 1 antibody, BMS-936558, ONO-4538) in patients with previously treated advanced non-small-cell lung cancer. *Journal of clinical oncology*. 2015;33(18):2004.

19. Kumar A, Sunita P, Jha S, Pattanayak SP. 7,8-Dihydroxycoumarin exerts antitumor potential on DMBA-induced mammary carcinogenesis by inhibiting ER α , PR, EGFR, and IGF1R: involvement of MAPK1/2-JNK1/2-Akt pathway. *Journal of Physiology and Biochemistry*. 2018;74(2):223-34.
20. Vinoth A, Kowsalya RJJoCR, Therapeutics. Chemopreventive potential of vanillic acid against 7, 12-dimethylbenz (a) anthracene-induced hamster buccal pouch carcinogenesis. 2018;14(6):1285.
21. Selby MJ, Engelhardt JJ, Johnston RJ, Lu L-S, Han M, Thudium K, et al. Preclinical development of ipilimumab and nivolumab combination immunotherapy: mouse tumor models, in vitro functional studies, and cynomolgus macaque toxicology. *PLoS One*. 2016;11(9):e0161779.
22. El-Mansy MN, Hassan MM, El-Nour A, Kholoud M, El-Hosary WH. Evaluation the safety of thymoquinone loaded on gold nanoparticles in the treatment of hamster buccal carcinogenesis. *Suez Canal University Medical Journal*. 2017;20(1):20-8.
23. Silvan S, Manoharan S. Apigenin prevents deregulation in the expression pattern of cell-proliferative, apoptotic, inflammatory and angiogenic markers during 7, 12-dimethylbenz [a] anthracene-induced hamster buccal pouch carcinogenesis. *Archives of oral biology*. 2013;58(1):94-101.
24. Parasuraman S, Zhen KM, Raveendran RJP, Toxicology, Reports B. Retro-orbital sample collection in Rats-a video article. 2015;1(2).
25. Faisal M, Abu Bakar M, Sarwar A, Adeel M, Batool F, Malik KI, et al. Depth of invasion (DOI) as a predictor of cervical nodal metastasis and local recurrence in early stage squamous cell carcinoma of oral tongue (ESSCOT). *PloS one*. 2018;13(8):e0202632.
26. Tsutsumi YJC. Pitfalls and caveats in applying chromogenic immunostaining to histopathological diagnosis. 2021;10(6):1501.
27. Desjobert C, El Mai M, Gerard-Hirne T, Guianvarc'h D, Carrier A, Pottier C, et al. Combined analysis of DNA methylation and cell cycle in cancer cells. 2015;10(1):82-91.
28. Baubec T, Schübeler DJCoig, development. Genomic patterns and context specific interpretation of DNA methylation. 2014;25:85-92.
29. Bruna F, Arango-Rodríguez M, Plaza A, Espinoza I, Conget P. The administration of multipotent stromal cells at precancerous stage precludes tumor growth and epithelial dedifferentiation of oral squamous cell carcinoma. *Stem Cell Research*. 2017;18:5-13.
30. Casto BC, Knobloch TJ, Galioto RL, Yu Z, Accurso BT, Warner BM. Chemoprevention of oral cancer by lyophilized strawberries. *Anticancer research*. 2013;33(11):4757-66.
31. El-Hossary WH, Hegazy E, El-Mansy MN. TOPICAL CHEMOPREVENTIVE EFFECT OF THYMOQUINONE VERSUS THYMOQUINONE LOADED ON GOLD NANOPARTICLES ON DMBA-INDUCED HAMSTER BUCCAL POUCH CARCINOGENESIS (IMMUNOHISTOCHEMICAL STUDY). *Egyptian Dental Journal*. 2018;64(4-October (Oral Medicine, X-Ray, Oral Biology & Oral Pathology)):3523-33.
32. Boeckx C, Baay M, Wouters A, Specenier P, Vermorken JB, Peeters M, et al. Anti-epidermal growth factor receptor therapy in head and neck squamous cell carcinoma: focus on potential molecular mechanisms of drug resistance. *The oncologist*. 2013;18(7):850-64.

33. Bonner JA, Harari PM, Giralt J, Azarnia N, Shin DM, Cohen RB, et al. Radiotherapy plus cetuximab for squamous-cell carcinoma of the head and neck. *New England Journal of Medicine*. 2006;354(6):567-78.
34. Vermorken JB, Mesia R, Rivera F, Remenar E, Kawecki A, Rottey S, et al. Platinum-based chemotherapy plus cetuximab in head and neck cancer. *New England Journal of Medicine*. 2008;359(11):1116-27.
35. Mohammed ES, Ahmed MM, Zouair MGA. Synergistic effect between cetuximab and curcumin on experimentally induced hamster buccal pouch carcinoma. *Al-Azhar Journal of Dental Science*. 2017, 20(2):145-52.
36. Lu Y, Li X, Liang K, Luwor R, Siddik ZH, Mills GB, et al. Epidermal growth factor receptor (EGFR) ubiquitination as a mechanism of acquired resistance escaping treatment by the anti-EGFR monoclonal antibody cetuximab. *Cancer research*. 2007;67(17):8240-7.
37. Khan A, Khan A, Shal B, Aziz A, Ahmed MN, Khan SJF, et al. N-(benzylidene)-2-((2-hydroxynaphthalen-1-yl) diazenyl) benzohydrazides (1-2)(NCHDH and NTHDH) attenuate DMBA-induced breast cancer via Nrf2/NF- κ B/apoptosis signaling. 2022.
38. Hassan MMA, Abd El Atif GA. EVALUATION OF DIFFERENTIAL MONOCYTES IN THE DMBA/HCP E CARCINOGENESIS MODEL UNDER THE INFLUENCE OF SOME PHYTOCHEMICAL AGENTS. *Egyptian Dental Journal*. 2017;63(2-April (Oral Medicine, X-Ray, Oral Biology & Oral Pathology)):1419-35.
39. Coffelt SB, Wellenstein MD, de Visser KEJNRC. Neutrophils in cancer: neutral no more. 2016;16(7):431-46.
40. Schernberg A, Blanchard P, Chargari C, Ou D, Levy A, Gorphe P, et al. Leukocytosis, prognosis biomarker in locally advanced head and neck cancer patients after chemoradiotherapy. 2018;12:8-15.
41. Chen Y-W, Chen I-L, Lin I-C, Kao S-Y. Prognostic value of hypercalcaemia and leucocytosis in resected oral squamous cell carcinoma. *British Journal of Oral and Maxillofacial Surgery*. 2014;52(5):425-31.
42. Hsieh L-T, Lin C-L, Chang Y-K, Ho S-YJJoMS. Paraneoplastic leukemoid reaction associated with poor prognosis in oral squamous cell carcinoma: A case report and literature review. 2020;40(1):42.
43. Granger JM, Kontoyiannis DP. Etiology and outcome of extreme leukocytosis in 758 nonhematologic cancer patients: a retrospective, single-institution study. *Cancer: Interdisciplinary International Journal of the American Cancer Society*. 2009;115(17):3919-23.
44. Kumar V, Sachan R, Rahman M, Rub RA, Patel DK, Sharma K, et al. Chemopreventive effects of *Melastoma malabathricum* L. extract in mammary tumor model via inhibition of oxidative stress and inflammatory cytokines. *Biomedicine & Pharmacotherapy*. 2021;137:111298.
45. Hamza AA, Khasawneh MA, Elwy HM, Hassanin SO, Elhabal SF, Fawzi NM. *Salvadora persica* attenuates DMBA-induced mammary cancer through downregulation oxidative stress, estrogen receptor expression and proliferation and augmenting apoptosis. *Biomedicine & Pharmacotherapy*. 2022;147:112666.
46. Deng Y, Ma M, Guo G, Tang ZJET. Kirenol regulates the cell proliferative and inflammatory markers in DMBA-induced oral squamous cell carcinogenesis in hamster. 2021;36(3):328-38.
47. Baskaran N, Manoharan S, Karthikeyan S, Prabhakar MM. Chemopreventive potential of coumarin in 7, 12-dimethylbenz [a] anthracene induced hamster

- buccal pouch carcinogenesis. *Asian Pacific Journal of Cancer Prevention*. 2012;13(10):5273-9.
48. Manoharan S, VasanthaSelvan M, Silvan S, Baskaran N, Singh AK, Kumar VV. Carnosic acid: a potent chemopreventive agent against oral carcinogenesis. *Chemico-biological interactions*. 2010;188(3):616-22.
 49. Anbalagan V, RAju K, ShAnMugAM M. Assessment of lipid peroxidation and antioxidant status in vanillic acid treated 7, 12-dimethylbenz [a] anthracene induced hamster buccal pouch carcinogenesis. *Journal of clinical and diagnostic research: JCDR*. 2017;11(3):BF01.
 50. Goubran HA, Elemetry M, Radosevich M, Seghatchian J, El-Ekiaby M, Burnouf TJCg, et al. Impact of transfusion on cancer growth and outcome. 2016;9:CGM. S32797.
 51. Ishida K, Tomita H, Nakashima T, Hirata A, Tanaka T, Shibata T, et al. Current mouse models of oral squamous cell carcinoma: genetic and chemically induced models. 2017;73:16-20.
 52. Chen P, Li X, Zhang R, Liu S, Xiang Y, Zhang M, et al. Combinative treatment of β -elemene and cetuximab is sensitive to KRAS mutant colorectal cancer cells by inducing ferroptosis and inhibiting epithelial-mesenchymal transformation. *Theranostics*. 2020;10(11):5107.
 53. Tao X, Lu Y, Qiu S, Wang Y, Qin J, Fan Z. AP1G1 is involved in cetuximab-mediated downregulation of ASCT2-EGFR complex and sensitization of human head and neck squamous cell carcinoma cells to ROS-induced apoptosis. *Cancer letters*. 2017;408:33-42.
 54. Lu H, Li X, Lu Y, Qiu S, Fan Z. ASCT2 (SLC1A5) is an EGFR-associated protein that can be co-targeted by cetuximab to sensitize cancer cells to ROS-induced apoptosis. *Cancer letters*. 2016;381(1):23-30.
 55. Ozkan A, Erdogan A, Ozkan O, Manguoglu E, Kiraz N. Enhanced anticancer effect of cetuximab combined with stabilized silver ion solution in EGFR-positive lung cancer cells. *Turkish Journal of Biochemistry*. 2019;44(4):426-37.
 56. Yang J, Mo J, Dai J, Ye C, Cen W, Zheng X, et al. Cetuximab promotes RSL3-induced ferroptosis by suppressing the Nrf2/HO-1 signalling pathway in KRAS mutant colorectal cancer. *Cell death & disease*. 2021;12(11):1-11.
 57. Swidan S, Hassan M, El-Hossary W. Chemopreventive effect of different doses of nanothymoquinone on chemically-induced oral carcinogenesis: Msc. Thesis., Suez Canal University; 2016.
 58. Baldasquin-Caceres B, Gomez-Garcia F, López-Jornet P, Castillo-Sanchez J, Vicente-Ortega V. Chemopreventive potential of phenolic compounds in oral carcinogenesis. *Archives of Oral Biology*. 2014;59(10):1101-7.
 59. Naveenkumar C, Raghunandhakumar S, Asokkumar S, Devaki T. Baicalein abrogates reactive oxygen species (ROS)-mediated mitochondrial dysfunction during experimental pulmonary carcinogenesis in vivo. *Basic & clinical pharmacology & toxicology*. 2013;112(4):270-81.
 60. Hussein AM, El-Sheikh SM, Darwish ZE, Hussein KA, Gaafar AI. Effect of genistein and oxaliplatin on cancer stem cells in oral squamous cell carcinoma: an experimental study. *Alexandria Dental Journal*. 2018;43(1):117-23.
 61. Mohammed ES, Ahmed MM, Zouair MGA. Synergistic effect between cetuximab and curcumin on experimentally induced hamster buccal pouch carcinoma.

62. Haidar Z, Fernández A, Fernández J, Marshall M, Martínez R, Niklander S. Difference in EGFR expression and mean vascular density in normal oral mucosa, oral epithelial dysplasia and oral squamous cell carcinoma. *Journal of Oral Research*. 2017;6(2):39-45.
63. Sarkis SA, Abdullah BH, Abdul Majeed BA, Talabani NG. Immunohistochemical expression of epidermal growth factor receptor (EGFR) in oral squamous cell carcinoma in relation to proliferation, apoptosis, angiogenesis and lymphangiogenesis. *Head & neck oncology*. 2010;2(1):1-8.
64. Rajeswari MRC, Saraswathi TR. Expression of epithelial growth factor receptor in oral epithelial dysplastic lesions. *Journal of oral and maxillofacial pathology: JOMFP*. 2012;16(2):183.
65. Rössle M, Weber CS, Züllig L, Graf N, Jochum W, Stöckli SJ, et al. EGFR expression and copy number changes in low T-stage oral squamous cell carcinomas. *Histopathology*. 2013;63(2):271-8.
66. Szabó B, Nelhübel GA, Kárpáti A, Kenessey I, Jóri B, Székely C, et al. Clinical significance of genetic alterations and expression of epidermal growth factor receptor (EGFR) in head and neck squamous cell carcinomas. *Oral oncology*. 2011;47(6):487-96.
67. Hou X, Yang F, Liu W, Fu Z, Chen L, Li Z, et al. Signaling pathways that facilitate chronic inflammation-induced carcinogenesis. *J Cell Signal*. 2015;1:9.
68. Dionysopoulos D, Pavlakis K, Kotoula V, Fountzilias E, Markou K, Karasmanis I, et al. Cyclin D1, EGFR, and Akt/mTOR pathway. Springer; 2013.
69. Freudlsperger C, Burnett JR, Friedman JA, Kannabiran VR, Chen Z, Van Waes C. EGFR-PI3K-AKT-mTOR signaling in head and neck squamous cell carcinomas: attractive targets for molecular-oriented therapy. *Expert opinion on therapeutic targets*. 2011;15(1):63-74.
70. Daniele S, Costa B, Zappelli E, Da Pozzo E, Sestito S, Nesi G, et al. Combined inhibition of AKT/mTOR and MDM2 enhances Glioblastoma Multiforme cell apoptosis and differentiation of cancer stem cells. *Scientific reports*. 2015;5(1):1-14.
71. Jafri SH, Glass J, Shi R, Zhang S, Prince M, Kleiner-Hancock H. Thymoquinone and cisplatin as a therapeutic combination in lung cancer: In vitro and in vivo. *Journal of Experimental & Clinical Cancer Research*. 2010;29(1):1-11.
72. Baumeister P, Heinrich K, Märte M, Reiter M, Schwenk-Zieger S, Harréus U. The impact of EGFR stimulation and inhibition on BPDE induced DNA fragmentation in oral/oropharyngeal mucosa in vitro. *Oral oncology*. 2011;47(12):1141-7.
73. Nakata Y, Uzawa N, Takahashi K-I, Sumino J, Michikawa C, Sato H, et al. EGFR gene copy number alteration is a better prognostic indicator than protein overexpression in oral tongue squamous cell carcinomas. *European Journal of Cancer*. 2011;47(15):2364-72.
74. Bernardes VF, Gleber-Netto FO, De Sousa SF, Rocha RM, De Aguiar MCF. EGFR status in oral squamous cell carcinoma: comparing immunohistochemistry, FISH and CISH detection in a case series study. *BMJ open*. 2013;3(1):e002077.

75. Dragomir L, Mărgăritescu C, Florescu A, Olimid A, Dragomir M, Popescu MJRME. The immunoeexpression of EGFR and Her2/neu in oral squamous carcinoma. 2012;53(3):597-601.
76. Theocharis S, Giaginis C, Dana E, Thymara I, Rodriguez J, Patsouris E, et al. Phosphorylated epidermal growth factor receptor expression is associated with clinicopathologic parameters and patient survival in mobile tongue squamous cell carcinoma. *Journal of Oral and Maxillofacial Surgery*. 2017;75(3):632-40.
77. Kriegs M, Clauditz TS, Hoffer K, Bartels J, Buhs S, Gerull H, et al. Analyzing expression and phosphorylation of the EGF receptor in HNSCC. *Scientific reports*. 2019;9(1):1-8.
78. Naruse T, Tokuhisa M, Yanamoto S, Sakamoto Y, Okuyama K, Tsuchihashi H, et al. Lower gingival squamous cell carcinoma with brain metastasis during long-term cetuximab treatment: A case report. *Oncology Letters*. 2018;15(5):7158-62.
79. Yin P, Cui S, Liao X, Yao X. Galectin-3 blockade suppresses the growth of cetuximab-resistant human oral squamous cell carcinoma. *Molecular medicine reports*. 2021;24(4):1-9.
80. Braig F, Kriegs M, Voigtlaender M, Habel B, Grob T, Biskup K, et al. Cetuximab resistance in head and neck cancer is mediated by EGFR-K521 polymorphism. *Cancer research*. 2017;77(5):1188-99.
81. Braig F, Voigtlaender M, Schieferdecker A, Busch C-J, Laban S, Grob T, et al. Liquid biopsy monitoring uncovers acquired RAS-mediated resistance to cetuximab in a substantial proportion of patients with head and neck squamous cell carcinoma. *Oncotarget*. 2016;7(28):42988.
82. Yonesaka K, Zejnullahu K, Okamoto I, Satoh T, Cappuzzo F, Souglakos J, et al. Activation of ERBB2 signaling causes resistance to the EGFR-directed therapeutic antibody cetuximab. *Science translational medicine*. 2011;3(99):99ra86-99ra86.
83. Napolitano S, Martini G, Rinaldi B, Martinelli E, Donniacuo M, Berrino L, et al. Primary and acquired resistance of colorectal cancer to anti-EGFR monoclonal antibody can be overcome by combined treatment of regorafenib with cetuximab. *Clinical Cancer Research*. 2015;21(13):2975-83.
84. Thaib, P. K. P., & Rahaju, A. S. (2022). Clinicopathological profile of clear cell renal cell carcinoma. *International Journal of Health & Medical Sciences*, 5(1), 91-100. <https://doi.org/10.21744/ijhms.v5n1.1846>
85. Schmitz S, Bindea G, Albu RI, Mlecnik B, Machiels J-P. Cetuximab promotes epithelial to mesenchymal transition and cancer associated fibroblasts in patients with head and neck cancer. *Oncotarget*. 2015;6(33):34288.
86. Ramu A, Kathiresan S, Ramadoss H, Nallu A, Kaliyan R, Azamuthu T. Gramine attenuates EGFR-mediated inflammation and cell proliferation in oral carcinogenesis via regulation of NF- κ B and STAT3 signaling. *Biomedicine & Pharmacotherapy*. 2018;98:523-30.
87. Kusama H, Shimoda M, Miyake T, Tanei T, Kagara N, Naoi Y, et al. Prognostic value of tumor cell DNA content determined by flow cytometry using formalin-fixed paraffin-embedded breast cancer tissues. 2019;176(1):75-85.
88. Quan H, Shan Z, Liu Z, Liu S, Yang L, Fang X, et al. The repertoire of tumor-infiltrating lymphocytes within the microenvironment of oral squamous cell carcinoma reveals immune dysfunction. 2020;69(3):465-76.

89. Lennartz M, Minner S, Brasch S, Wittmann H, Paterna L, Angermeier K, et al. The Combination of DNA Ploidy Status and PTEN/6q15 Deletions Provides Strong and Independent Prognostic Information in Prostate Cancer DNA Ploidy and PTEN/6q15 Deletions in Prostate Cancer. 2016;22(11):2802-11.
90. Hussein AM, Zahran AM, Badawy M, Gobran HG, Edrees MF, Omar EMJIJDOS. The Role of CD44 Cancer Stem Cell Marker in the Development and Progression of Lymph Node Metastasis in Oral Squamous Cell Carcinoma. 2021;8(11):4917-22.
91. El-Deftar M, El Gerzawi S, Abdel-Azim A, Tohamy SJJotENCI. Prognostic significance of ploidy and S-phase fraction in primary intraoral squamous cell carcinoma and their corresponding metastatic lymph nodes. 2012;24(1):7-14.
92. Zahran A, Fakhry H, Hussein K, Abd El-Salam M, Mohamed M, Tohamy SJCO. Flow cytometry analysis of DNA ploidy and S-phase fraction in salivary gland tumors of Egyptian patients. 2018;3:1393-8.
93. Suryasa, I. W., Rodríguez-Gámez, M., & Koldoris, T. (2022). Post-pandemic health and its sustainability: Educational situation. *International Journal of Health Sciences*, 6(1), i-v. <https://doi.org/10.53730/ijhs.v6n1.5949>
94. Otsuka A, Dummer RG. New Therapies and Immunological Findings in Melanoma and Other Skin Cancers: *Frontiers Media SA*; 2019.
95. Badr El-Din NK, Ali DA, Alaa El-Dein M, Ghoneum M. Enhancing the apoptotic effect of a low dose of paclitaxel on tumor cells in mice by arabinoxylan rice bran (MGN-3/Biobran). *Nutrition and cancer*. 2016;68(6):1010-20.